

Double Bionic Deformable DNA Hydrogel Microneedles Loaded with Extracellular Vesicles to Guide Tissue Regeneration of Diabetes Ulcer Wound

Liping Zhou, Zehua Zeng, Jingchong Liu, Fengshi Zhang, Xiaochun Bian, Zhiwei Luo, Hongwu Du,* Peixun Zhang,* and Yongqiang Wen*

Due to the high blood glucose and low oxygen environment in diabetes wounds, complex pathological problems arise, such as failure to upregulate healing factors, biological barriers generation, microvascular lesions, and skin neuropathy. Inspired by nature and traditional Chinese paper-cutting technology, polypeptide deoxyribonucleic acid (DNA) hydrogel microneedles (MNs) (P-DNA gel MNs) are prepared. The obtained P-DNA gel MNs possess optimized structure and large deformability, providing excellent clamping, stability, skin penetration, large deformation, tissue adhesion, and antibacterial properties. By incorporating extracellular vesicles (EVs) extracted under hypoxia (H-EVs-hypoxia), P-DNA gel MNs can regulate tissue microenvironment, scavenge free radicals, and reduce inflammation. Notably, P-DNA gel MNs integration system activates immune regulation and beneficial pathways, promoting neurogenesis and angiogenesis, reducing pathological pain, and achieving high-quality healing. Overall, P-DNA gel MNs system presents a fundamental mechanism for clinical transformation in treating diabetes wounds.

1. Introduction

Chronic wounds, especially ulcerative wounds in diabetes, remain thorny problems. World Health Organization (WHO) estimates that by 2045, 25% of 629 million diabetes patients will face lifelong chronic nonhealing wounds.^[1a,b] Hyperglycemia and oxidative stress^[1a] cause various systemic disease symptoms^[1b] in diabetes patients, such as low immunity,^[1c] bacterial infection,

high expression of inflammatory factors, excessive reactive oxygen species (ROS) production, inability to upregulate healing factors, pain signals activation, microvascular and peripheral neuropathy.^[1–3] Dysfunctional stromal cells are the primary cause of nonhealing or delayed healing, leading to pathological lesions and system damage.^[3] Ideal dressing should comprehensively address the complex pathological problems of wounds and actively promote the participation of various cells in regeneration.

Guided tissue regeneration uses endogenous cells stimulated by extracellular signals or reprogrammed by intracellular biomolecules.^[4] Stem cells are commonly used in this process because their multi-directional differentiation and self-renewal.^[5–7] Pluripotent stem cells in hair follicles have great potential because they

can become various functional cells, such as adipocytes, osteoblasts, chondrocytes, neural and glial cells.^[8] Compared with other mesenchymal stem cells, hair follicles are abundant, easy to get, less harmful to body, and accepted by patients.^[8a,b] However, stem cell use has limits due to immune rejection and cell viability. Stem cells did wound repair and regeneration through paracrine-secreted extracellular vesicles (EVs).^[8c] EVs have low immune rejection, high stability, easy storage, inherent homing effect, and effective molecular signal transmission.^[8c] However, high glucose and hypoxia diabetes microenvironment challenge EVs in the wound repair, such as maintaining sufficient vitality, function, effective targeting, and sustained release.

Biomaterials were designed for manufacturing dressings with specific wound repair properties.^[2,9] Compared with traditional polymers, deoxyribonucleic acid (DNA) is a natural biopolymer material. Number and arrangement order of DNA units can be precisely customized as desired.^[10–12] Modifiability of DNA units also endows it with multifunctionality.^[12] Therefore, DNA's base pairing and self-assembly abilities make it a unique material for building bridging biology, polymer, and tissue engineering.^[13a] DNA hydrogel, a three-dimensional polymer network with DNA as its structural unit, combines the benefits of hydrogel's skeleton structure and DNA's biological characteristics.^[13b] This integration provides platform for bioactive substances and enables material functionalization.^[14]

Diabetes patients with skin defects or open are at higher risk of infections due to their immunity.^[15a,b] Drug-resistant

L. Zhou, Z. Zeng, J. Liu, X. Bian, Z. Luo, H. Du, Y. Wen
 Beijing Key Laboratory for Bioengineering and Sensing Technology
 Daxing Research Institute
 School of Chemistry and Biological Engineering
 University of Science and Technology Beijing
 Beijing 100083, China
 E-mail: hongwudu@ustb.edu.cn; wyq_wen@ustb.edu.cn

L. Zhou, F. Zhang, P. Zhang
 Department of Orthopaedics and Trauma
 Peking University People's Hospital
 Peking University
 Beijing 100044, China
 E-mail: zhangpeixun@bjmu.edu.cn

 The ORCID identification number(s) for the author(s) of this article can be found under <https://doi.org/10.1002/adfm.202312499>

[Correction added on January 26, 2024, after first online publication: Hongwu Du and Peixun Zhang have been assigned as corresponding authors in this version.]

DOI: [10.1002/adfm.202312499](https://doi.org/10.1002/adfm.202312499)

bacteria can form biofilm at the wound site, making it difficult for the drug to penetrate and work. Also, bacteria migrating to subcutaneous tissue can cause more damage. Microneedles (MNs) have gained attention for their minimally invasive nature, ability to overcome barriers, and accurate sustained drug release.^[16–18] However, traditional vertically aligned MNs have difficulty overcoming skin tension, leading to wound rupture or enlargement during recovery.^[19,20a] Most reported^[20b] MNs are conical and smooth, resulting in weak adhesion and usually requiring additional suture fixation. Inspired by the bidirectional nature structures of crab claw^[20c] and shark microgroove,^[20d] MNs could be realized through structural design to enhance the grasping force and reduce implant resistance, and increase pull-out resistance to prevent wound rupture and improve the fit. Otherwise, the current non-deformable MN caps pose challenges for joint wounds. By drawing inspiration from traditional Chinese paper-cutting technology,^[20e] the design of MNs caps with large deformation structures is expected to address this issue. Therefore, developing diversified MNs with unique designs and functions is an effective strategy.

Taking inspiration from crab claw, shark microgroove structure, and traditional Chinese paper-cutting technology, we designed double bionic and large deformable DNA gel MNs (**Scheme 1**). Polypeptide or Catechol-Polypeptide DNA segments (P-A₁ or C-P-A₂ DNA segments), the other DNA segments (B/C/D segments), and EVs were mixed and injected into 3D printed mold to form the polypeptide-DNA hydrogel MNs (P-DNA gel MNs). P-DNA gel MNs were formed by DNA base pairing, covalent bond crosslinking, and physical entanglement (**Scheme 1a**). Double bionic structures gave the MNs crab claw-like, flat, inclined structures, and shark microgroove structures, which improved stability, grasp force, and reduced resistance when entering the skin. Large deformation structure improves the comfort of patients' joint wounds. We evaluated the performance of P-DNA gel MNs, including stability, adhesion, deformation, antibacterial performance, biocompatibility, and antioxidant capacity (**Scheme 1b**). Through full-thickness tissue defect, transcriptome sequencing, and histology, we explored how P-DNA gel MNs guide macrophage polarization, reduce pain, and accelerate vascular neurogenesis to improve wound healing (**Scheme 1c**). Overall, P-DNA gel MNs integration dressing system activates beneficial pathways that regulate wound microenvironment and promote high-quality wound healing.

2. Discussion and Analysis

2.1. Characterization of the P-DNA Gel MNs

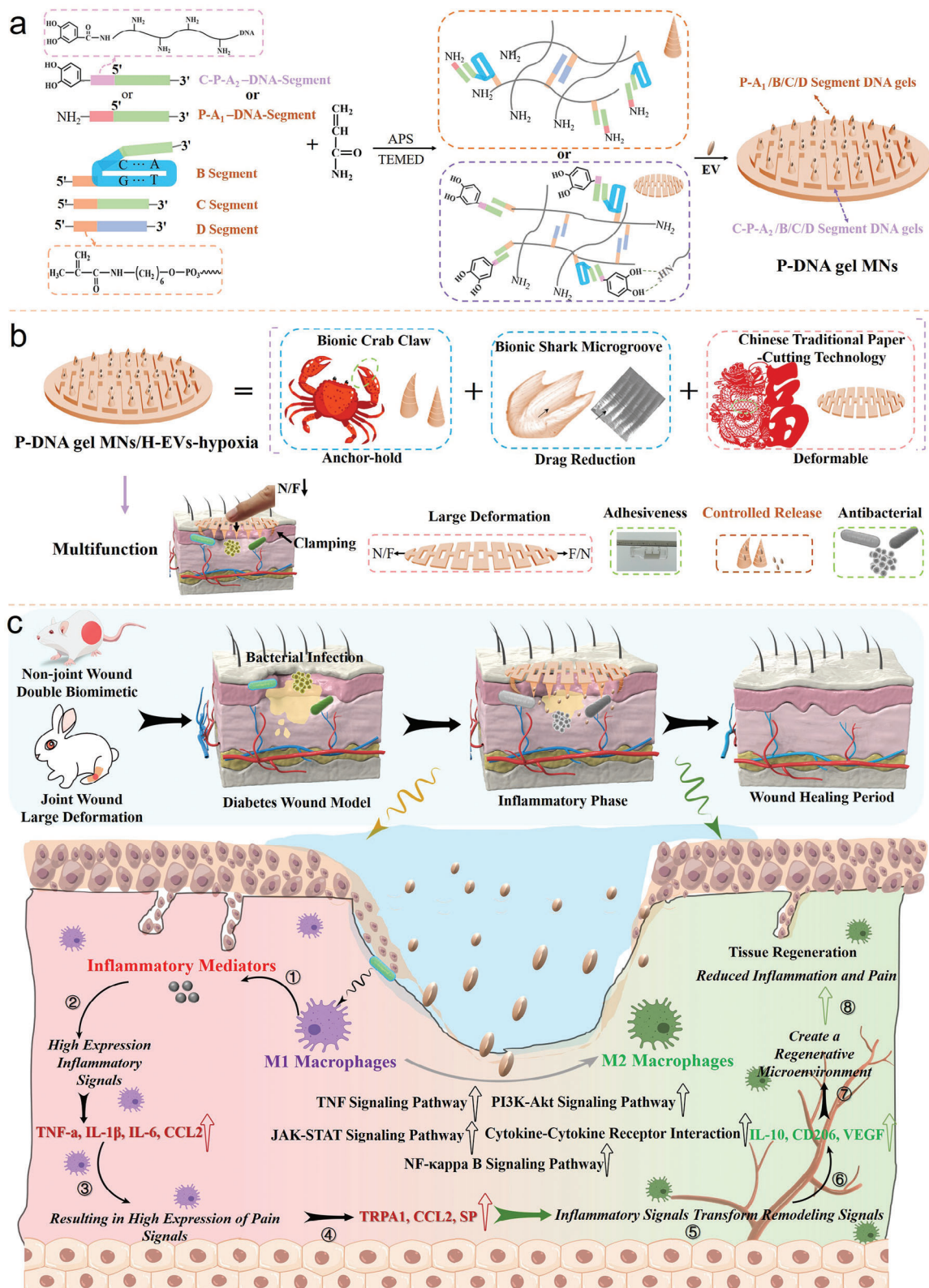
To penetrate the skin, MNs require a force >0.058 N per needle.^[21,22] We utilized the design and modifiability of DNA segments to achieve penetration through the skin^[23] (**Figure S1a**, Supporting Information). Anion mass spectrometry analysis confirmed the relative molecular mass of the target product, P-A₁-DNA segment, to be Mw: 8668.00 g mol⁻¹ (**Figure S1b**, Supporting Information). The single ultraviolet (UV) absorption peak also confirmed the successful synthesis of the target product (**Figure S1c**, Supporting Information). We modified polypeptide K-terminus with 3,4-dihydroxyphenylacetic acid to endow DNA polymer inherent adhesiveness (**Figure S2a**, Sup-

porting Information). C-P-A₂-DNA segment with the bisphenol hydroxyl group was assembled by Michael's addition reaction with the catechol-polypeptide (C-P) and A₂-DNA segment (**Figure S2b**, Supporting Information). Anionic mass spectrometry and singleUV absorption peak confirmed its successful synthesis (**Figure S2c,d**, Supporting Information). P-DNA gel MNs were formed by injecting P-A₁/B/C/D DNA segment solution into 3D printed mold MNs needles (**Table S2**, Supporting Information) and C-P-A₂/B/C/D DNA segment solution into the MNs cap region (**Table S3** and **Figure S3**, Supporting Information). The interaction of Watson Crick, Hoogsteen, and dense hydrogen bonds facilitated the formation of P-DNA gel MNs. Double bionics structures and paper-cutting technology endow P-DNA gel MNs with clamping, reducing resistance, and large deformation (**Figure 1a**) (Note: 3D printed mold was designed with double bionic structures and paper-cutting technology).

P-DNA gel MNs macro-morphology was observed under the high-definition electron microscope and found to resemble crab claws (**Figure 1b**). The microgroove structure was similar to shark microgroove using a scanning electron microscope (SEM) (**Figure 1c**). Tests using a universal tester showed that MNs with microgroove structure had a smaller insertion force per unit area than those without (**Figure S4a**, Supporting Information). This indicates that the microgroove structure reduces resistance when the MNs penetrate the skin and improves the pull-out force, enhancing skin adhesion (**Figure S4b**, Supporting Information). To evaluate the mechanical strength of P-DNA gel MNs, we conducted compression experiments. When the sensor reached position it started calculating the force and continued moving 0.3 mm. The micromorphology changed before and after stressing P-DNA gel MNs (**Figure 1d**). Mechanical strength (**Figure 1e**) and Young's modulus (**Figure S4c**, Supporting Information) of MNs increased with increase in concentration, indicating higher resistance to deformation.

Dressing with inherent adhesion can reduce the cumbersome procedure of dressing wound.^[2] The P-DNA gel MNs cap can adhere to glass, aluminum products, and plastic (**Figure S4d**, Supporting Information) because catechol groups modified on DNA segments can bind to thiols, amines, and imidazole groups on tissue surface proteins^[24a,b] and the A and T in the DNA unit can provide physical cross-linking through the hydrogel between them to ensure adhesion to the solid surface.^[24c,2a] When concentration reached 10%, it can adhere to 200 g weight (**Figure S4e**, **Movie S1**, Supporting Information). MNs exhibited optimum adhesion with porcine muscle (14.63 ± 0.4 Kpa) (**Figure S4f**, Supporting Information). Tests on skin tissue showed that MNs remained firmly attached even when volunteers moved their finger joints back and forth. Upon removal, there were no traces or redness left behind (**Figure 1f** and **Movie S2**, Supporting Information). Visualization dressings provided guidance for doctors to change dressings. The transmittance of MNs exceeded 89.8% and concentration change did not affect visualization (**Figure S5a**, **Movie S3**, Supporting Information).

Ulcerative wounds inevitably occur at joints so elastic deformation dressing could meet the joints' comfort.^[2] We evaluated the tensile properties of P-DNA gel MNs cap and found that MNs cap with a larger deformation had a smaller tensile slope but a more extensive strain (**Figure S5b**, Supporting Information). MNs cap with a 10% concentration had excellent stretching and



Scheme 1. a) P-DNA gel MNs synthesis process. b) Multifunctional properties of P-DNA gel MNs. c) Overall evaluation of wound microenvironment in diabetes after treatment with P-DNA gel MNs/H-EVs hypoxia.

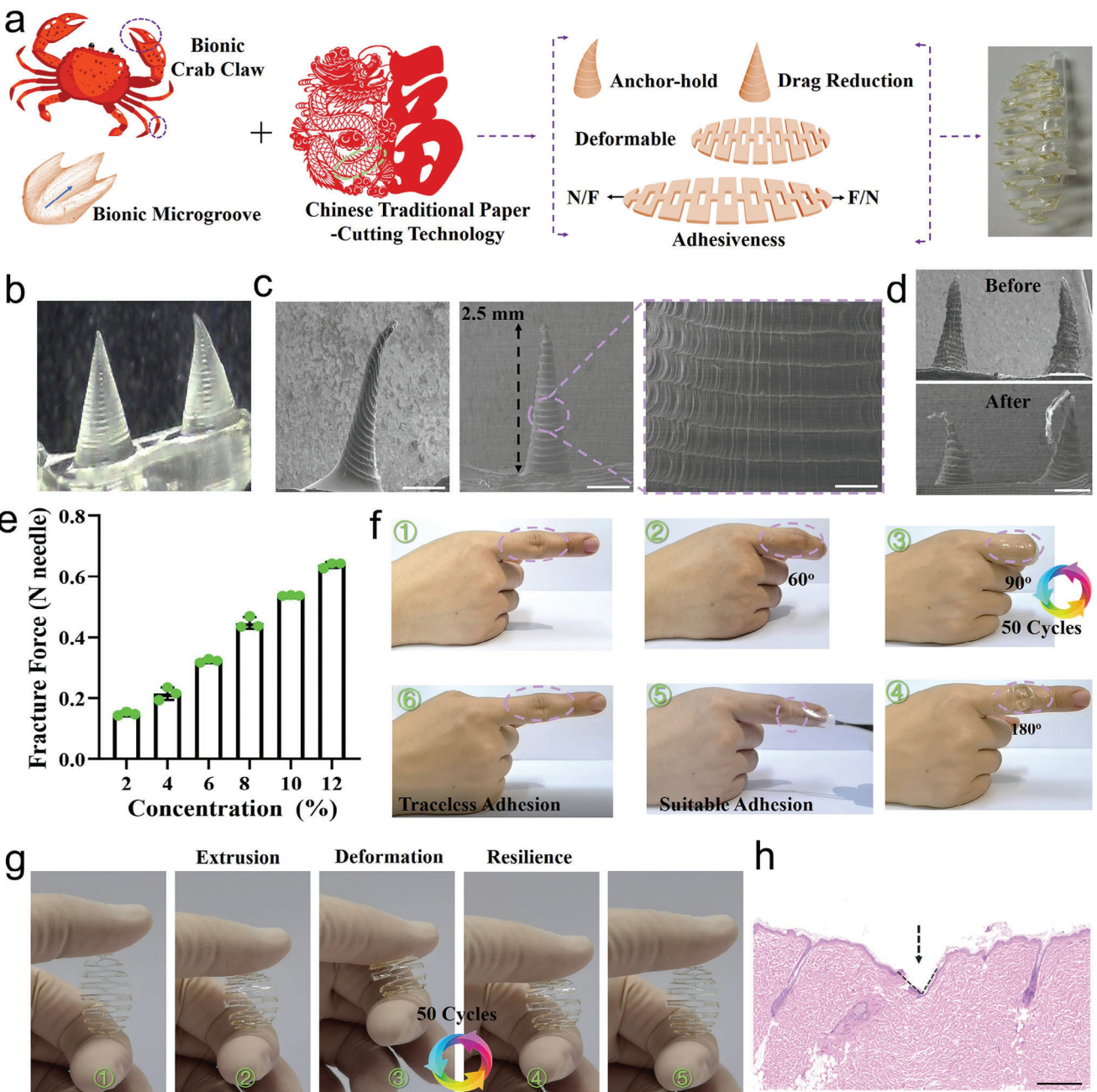


Figure 1. Morphology and characteristics of P-DNA gel MNs. a) Mechanism diagram of bionic characteristics of P-DNA gel MNs. b) Macrostructure of P-DNA gel MNs. c) Microstructure of P-DNA gel MNs (Scale bar: 1 mm and 200 μ m). d) Scanning electron microscope (SEM) images of P-DNA gel MNs before and after the mechanical strength test (Scale bar: 500 μ m). e) The fracture forces of the MNs with different P-DNA gel concentrations. f) P-DNA gel MNs cap adhesion effect on joints. g) Large deformation of P-DNA gel MNs. h) Microscopy images of H&E staining of sectioned mouse skin after applying P-DNA gel MNs (Scale bar: 5 mm).

elastic deformation properties (Figure S5c, Supporting Information) and macro tensile and shrinkage behaviors (Figure S5d, Movie S4, Supporting Information). MNs caps could recover their original shape even after 50 cycles of 120° bending deformation (Figure 1g, Movie S5, Supporting Information). Dynamic crosslinking endowed MNs caps with high tensile strength and recoverability and provided strong and reliable guarantee for treating joint wounds. Due to excessive tissue fluid in ulcerative

wounds, we evaluated the absorption expansion rate of P-DNA gel MNs and found that the swelling rate decreased with the increase in concentration (Figure S6a, Supporting Information). We also evaluated biodegradability by calculating the dry-weight ratio.^[24d] MNs caps with 2% and 4% concentrations degraded rapidly, while those with 12% concentration had a lower degradation rate due to their high crosslinking density (Figure S6b, Supporting Information). Considering comprehensively above,

we selected 10% MNs to penetrate the skin, and hematoxylin-eosin staining demonstrated successful penetration through the stratum corneum (Figure 1h). Compared with ordinary dressings, DNA MN's inherent puncture ability could be fixed to wounds with blood clots and adipose tissue.

2.2. Characterization and Identification of H-EVs-Hypoxia

EVs could regulate the physiological and pathological microenvironment of wound, such as immune polarization, angiogenesis, and neurogenesis.^[24–28a] Unlike traditional stem cell therapy, EVs offer advantages such as high stability, accessibility, and easy storage.^[28b,c] To ensure that EVs play a functional role in the anaerobic environment of chronic wounds, we obtain EVs from hair follicle stem cells under hypoxia (HFSCs, H-EVs-hypoxia). We characterized the morphology of H-EVs-hypoxia using transmission electron microscopy (TEM) and found them to be spherical, round, or cup-shaped with a diameter of 126 ± 14.2 nm (Figure 2a,b). To verify the successful acquisition of EVs, we analyzed the protein expression of TSG101, CD9, and CD63 by Western blot (WB) (Figure 2c). The results indicated that H-EVs-hypoxia had typical morphological and molecular characteristics. Since wound healing was related to the mutual regulation of various cells, the successful transport of H-EVs-hypoxia to the critical cells involved in the regulation was a prerequisite for treating the wound healing mechanism.^[28] H-EVs-hypoxia were stained with PKH-26 red fluorescence by membrane labeling technology.^[24] Confocal micrographs showed that the number of H-EVs-hypoxia attachments and internalization in Normal Human Dermal Fibroblast (NHDF) cells gradually increased (Figure 2d and Figure S7a, Supporting Information). Furthermore, flow cytometry results also demonstrated this (Figure S7b, Supporting Information).

2.3. Antibacterial Properties of P-DNA Gel MNs

Post-traumatic infection has always been inevitable in healing, especially in diabetes patients with low immunity and vulnerability to bacterial invasion.^[28c,29] Cationic peptides can effectively disturb the bacterial membrane, leading to bacterial contents leakage and eventual bacterial death.^[30,31a] We assessed antibacterial mechanism (Figure S8, Supporting Information) and the antibacterial activities of H-EVs-hypoxia, P-DNA gel MNs (Figure S9a, Supporting Information), and P-DNA gel MNs/H-EVs-hypoxia (Figure S10a, Supporting Information) for *Staphylococcus aureus* (*S. aureus*), *Escherichia coli* (*E. coli*), and *Pseudomonas aeruginosa* (*P. aeruginosa*) using the agar diffusion assay method. H-EVs-hypoxia demonstrated low antibacterial activity, while P-DNA gel MNs (3 mMmm) exhibited excellent antibacterial properties (Figure S9b–d, Supporting Information). Antibacterial rate of P-DNA gel MNs/H-EVs-hypoxia (3 mM mm) was $98\text{--}99 \pm 0.4\%$ (Figure S10b–d, Supporting Information). The decrease in bacterial activity at 2.2 and 2.6 mM mm might be attributed to the molar concentration of the polypeptide chain.

To further confirm the excellent antibacterial ability of P-DNA gel MNs/H-EVs-hypoxia, the bacteria morphologies were observed by SEM. P-DNA gel MNs/H-EVs-hypoxia effectively dis-

rupted the bacterial membrane's integrity (Figure S11, Supporting Information), leading to efficient destruction, osmotic dissolution of cell transmembrane potential, and ultimately bacteria death.^[31b] Control group exhibited complete membrane structure. TEM also confirmed that bacterial membrane shape was irregular, and intracellular organelles were damaged, resulting in membrane integrity cracking and intracellular molecular leakage (Figure S12, Supporting Information). Bacterial viability was further evaluated by Live/dead staining. When the bacterial membrane was disrupted, PI stained the bacteria red, while SYTO9 dyed the complete bacterial membrane green. After incubation with P-DNA gel MNs/H-EVs-hypoxia (3 mM mm), the three bacteria were stained red while control group bacteria were green (Figures S13 and S14, Supporting Information). The above results indicate that P-DNA gel MNs/H-EVs-hypoxia has excellent antibacterial effects.

2.4. Biocompatibility, Proliferation, Migration, and Differentiation of the P-DNA Gel MNs/H-EVs-Hypoxia In Vitro

Wound dressings that come into direct contact with skin tissue should have excellent biocompatibility and promote the biological behavior of cells.^[32] To evaluate the toxicity of different materials, we conducted CCK8 test, which showed that P-DNA gel MNs at a concentration of 6.25 mg mL^{-1} had a cell survival rate of over 96.4% (Figure S15, Supporting Information). Diabetes patients are prone to vascular damage, which can impede oxygen delivery to wounds and create an anoxic environment that is exacerbated by the recruitment of inflammatory cells with high oxygen consumption.^[2b] However, stem cells express hypoxia-inducible factor-1 α (HIF-1 α) and can adapt to the hypoxic environment, increasing their vitality, enhancing their autocrine ability, maintaining stemness, and reducing cell apoptosis.^[2] Additionally, exosomes secreted in a hypoxic environment can promote cell proliferation, migration, and macrophage polarization.^[32] We evaluated the activity of EVs in promoting cell proliferation under different conditions. While there was no significant difference between H-EVs-normal and H-EVs-hypoxic in promoting cell proliferation at 12 h (Figure S16a, Supporting Information), H-EVs-hypoxic promoted cell proliferation to magnitude higher than H-EVs-normal after 24 h (Figure S16b, Supporting Information). This indicated that H-EVs-hypoxia initiates program to promote cell proliferation. Then, we evaluated the toxicity of different materials with Live/death staining kit and did not observe cell death (Figure S17a,b, Supporting Information). The hemolysis rates of the different materials were almost low 0.8% (Figure S17c, Supporting Information). Excellent biocompatibility ensured the possibility of P-DNA gel MNs as wound dressings.

Wound healing is dependent on cell proliferation, migration, and differentiation, which can be facilitated by functional biomaterials that activate biological behavior.^[2a] We co-cultured materials with NIH3T3 cells and observed the cell growth states. Compared with other three groups, P-DNA gel MNs/H-EVs-hypoxia could quickly promote cell growth (Figure S18a,b, Supporting Information). SEM also showed that this group proliferated faster than other groups (Figure S19a, Supporting Information). Furthermore, P-DNA gel MNs/H-EVs-hypoxia group promoted cell migration in a scratch assay, completing migration within 24 h

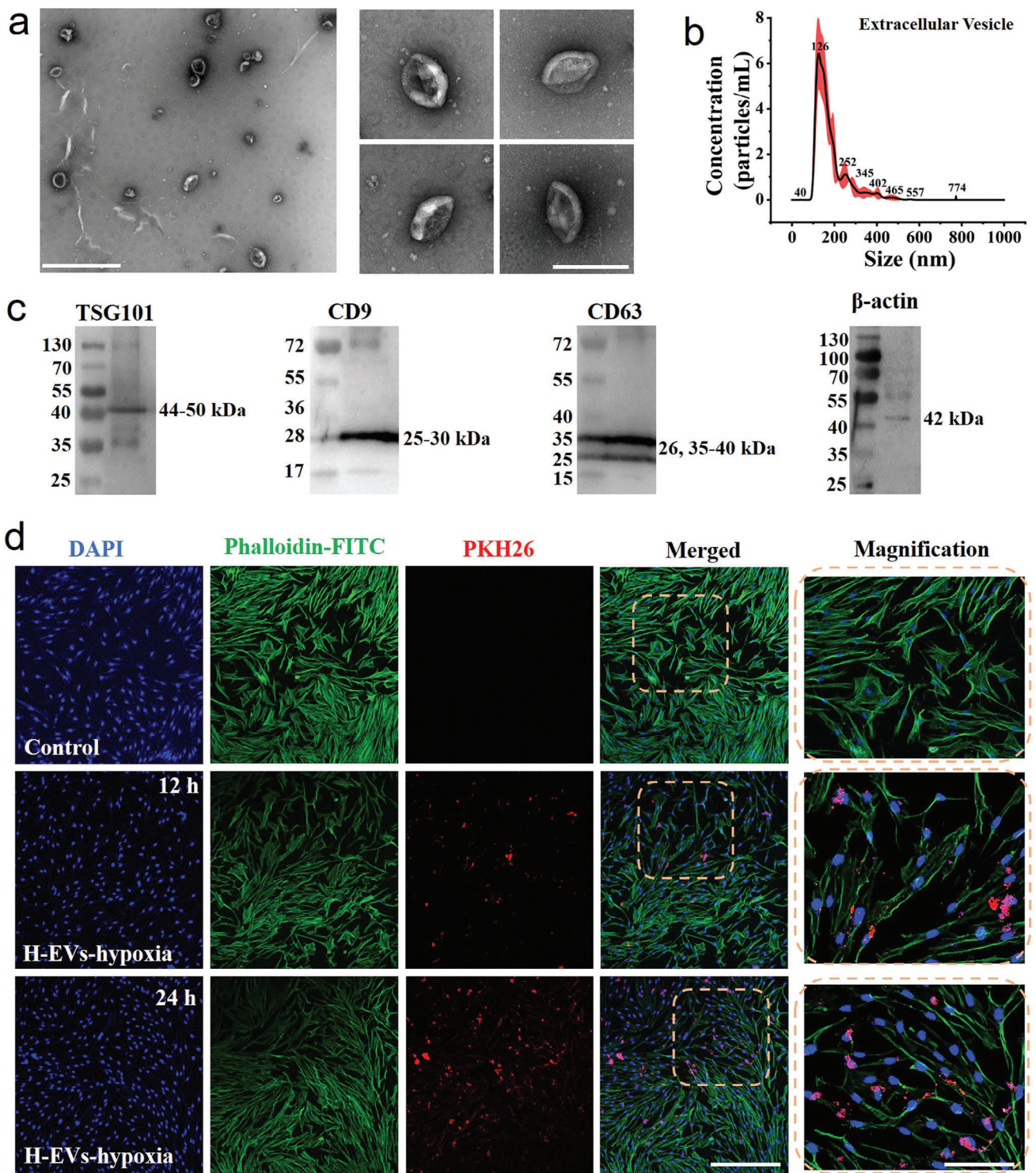


Figure 2. Characterization and identification of H-EVs-hypoxia. a) TEM image of H-EVs-hypoxia (scale bar: 500 nm and 200 nm). b) Nanoparticle analysis size distribution ($n = 3$). c) Presence of H-EVs-hypoxia surface marker proteins. d) Uptake of H-EVs-hypoxia by NHDF cells (scale bar: 100 nm and 200 nm).

(Figure S19b,c, Supporting Information). Since high hypoxia diabetes wounds can inhibit angiogenesis and impair healing,^[2] we investigated whether EVs in the hypoxic environment could promote the migration and proliferation of vascular endothelial cells (HUVEC). Using Trans well and cell-flow assay, we found that P-DNA gel MNs/H-EVs-hypoxia group had significantly higher rates of cell migration and proliferation compared to other groups, with rates 1.9–3.2 times higher (Figure S20a,b, Supporting Information) and 1.4–2.1 times higher, respectively (Figure S20c, Supporting Information). Otherwise, Rat Schwann cells (RSC) induced by P-DNA gel MNs/H-EVs-hypoxia showed a gradual shift toward filopodial processes morphology (Figure S21a,b, Supporting Information), indicating potential for neurological function recovery and nerve axon shaping. Combination of guiding biological development of DNA and H-EVs-hypoxia was more conducive to regulating cell biological behavior.

Diabetes wounds can cause ulceration due to the production of excessive ROS.^[2a] Previous reports show that EVs therapy could improve antioxidant capacity in oxidative stress-induced cell and skin damage.^[32] To evaluate the efficacy of H-EVs-hypoxia therapy in addressing excessive Reactive Oxygen Species (ROS) in diabetes wounds, we used 2,7-Dichlorodi-hydrofluorescein diacetate (DCFH-DA) to activate ROS and emit fluorescence. Compared with other groups, fluorescence quenching was significant in H-EVs-hypoxia and P-DNA gel MNs/H-EVs-hypoxia groups, indicating the system was expected to solve ROS phenomenon in diabetes wounds (Figure S22a,b, Supporting Information).

2.5. Inflammatory Polarization of the P-DNA Gel MNs/H-EV-Hypoxia In Vitro

In diabetes ulcer wounds, macrophages were spontaneously difficult to change from proinflammatory M1 to repairability M2.^[32] Biomaterials, growth factors, active substances, and EVs with specific biochemical properties may regulate their polarization.^[2,32,33] To evaluate the anti-inflammatory effect of material co-cultured with lipopolysaccharide (LPS)-induced RAW 264.7 cells, we monitored macrophage polarization over 24 h.^[2] Inflammatory factors (TNF- α and IL-1 β) were significantly decreased after H-EVs-hypoxia and P-DNA gel MNs/H-EVs hypoxia treatment in 12 h (Figure S23a,b, Supporting Information). After 24 h, the inflammatory factors were almost undetectable (Figure S24a,b, Supporting Information). Additionally, ELISA has also demonstrated that H-EVs-hypoxia and P-DNA gel MNs/H-EVs hypoxia can significantly reduce IL-1 β and IL-6 inflammation (IL-1 β : 211.26 pg mg⁻¹ for control, 107.40 pg mg⁻¹ for H-EVs-hypoxia, and 69.94 pg mg⁻¹ for P-DNA gel MNs/H-EVs hypoxia (Figure S25a, Supporting Information); IL-6: 271.23 pg mg⁻¹ for control, 131.48 pg mg⁻¹ for H-EVs-hypoxia, and 97.32 pg mg⁻¹ for P-DNA gel MNs/H-EVs hypoxia (Figure S25b, Supporting Information)). Notably, H-EVs-hypoxia induced a more significant anti-inflammatory effect compared to the H-EVs-normal group due to cell-derived EVs being conducive to inducing M2 macrophage polarization under hypoxic conditions.^[32–34]

The mRNA expression of anti-inflammatory factor IL-10 significantly increased after treatment with H-EVs-hypoxia and P-DNA gel MNs/H-EVs-hypoxia for 12 h (Figure S26a, Sup-

porting Information), and IL-10 expression was 9.2–9.3 and 7.2–7.4 times higher than the control group after 24 h (Figure S26b, Supporting Information). IL-10 was known as the symbol of anti-inflammatory and repairing polarization of M2 phenotype.^[2,33] Cellular immunofluorescence also showed that anti-inflammatory fluorescence intensity of H-EVs-hypoxia group was higher than that of H-EVs-normal group, indicating that H-EVs in the hypoxic environment are more effective in converting macrophages to repair phenotype (Figure S27a, Supporting Information). The M2 polarization rate^[35] of P-DNA gel MNs/H-EVs-hypoxia group was the most significant (Figure S27b, Supporting Information). Additionally, the H-EVs-hypoxia group treatment intensely increased the expression level of IL-10 (Figure S28a, Supporting Information) and TGF- β 1 (Figure S28b, Supporting Information) to 44.37 and 184.05 pg mg⁻¹, significantly higher than that in the H-EVs-normal group by ELISA analysis (38.44 and 162.87 pg mg⁻¹). Otherwise, the Flow cytometry analysis^[35b] showed that the number of CD206⁺ cell in the P-DNA gel MNs/H-EVs-hypoxia group increased by over 9.15% compared with the control group (Figure S29a–e, Supporting Information). Overall, P-DNA gel MNs/H-EVs-hypoxia enhanced proliferation and immune regulatory capacity.

2.6. Application of Different Materials in Diabetes Ulcer Wounds and Joint Wounds

We evaluated the efficacy of different materials in promoting the healing of full-thickness diabetes wounds infected with *P. aeruginosa*. The diabetes wound treatment details are described in Figure 3a. After the mice were induced into diabetes model, we randomly divided them into 7 groups and monitored body weight (Figure S30a, Supporting Information) and blood glucose (Figure S30b, Supporting Information) throughout the treatment period to assess their physiological status. According to the animal theory of the People's Hospital of Peking University, we evaluated the antibacterial properties of different materials in vivo on the 2nd day after treatment. P-DNA gel MNs/H-EVs hypoxia have excellent antibacterial properties, with an antibacterial rate of up to 99.8 ± 0.2% (Figure S31, Supporting Information).

At different time points, we monitored and photographed the wounds. The ordinary straight P-DNA gel MNs-1 caused wound rupture and enlargement on treatment two days (Figure 3b). The wound of P-DNA gel MNs with optimized structure (double bionic and large deformation structure) was significantly smaller than without. In the control and H-EVs-hypoxia groups, ulcers and decay appeared on the 4th day, along with bacterial cross-infection due to the lack of antibacterial ability (Figure S32, Supporting Information). Although the inherent antibacterial property and adsorbed tissue fluid of the P-DNA gel MNs group made the wound begin to scab on the 4th day, the healing effect was significantly lower than P-DNA gel MNs/H-EVs-hypoxia due to the lack of nutrients-H-EVs-hypoxia. P-DNA gel MNs/H-EVs-hypoxia group wound entered the healing state after treatment.

On the 22nd day, P-DNA gel MNs/H-EVs-hypoxia group was almost wholly healed (Figure S33a, Supporting Information) due to the double bionic and large deformation structure (Figure S33b, Supporting Information) and H-EVs-hypoxia endowing nutrients. Statistical analysis revealed that the wounds

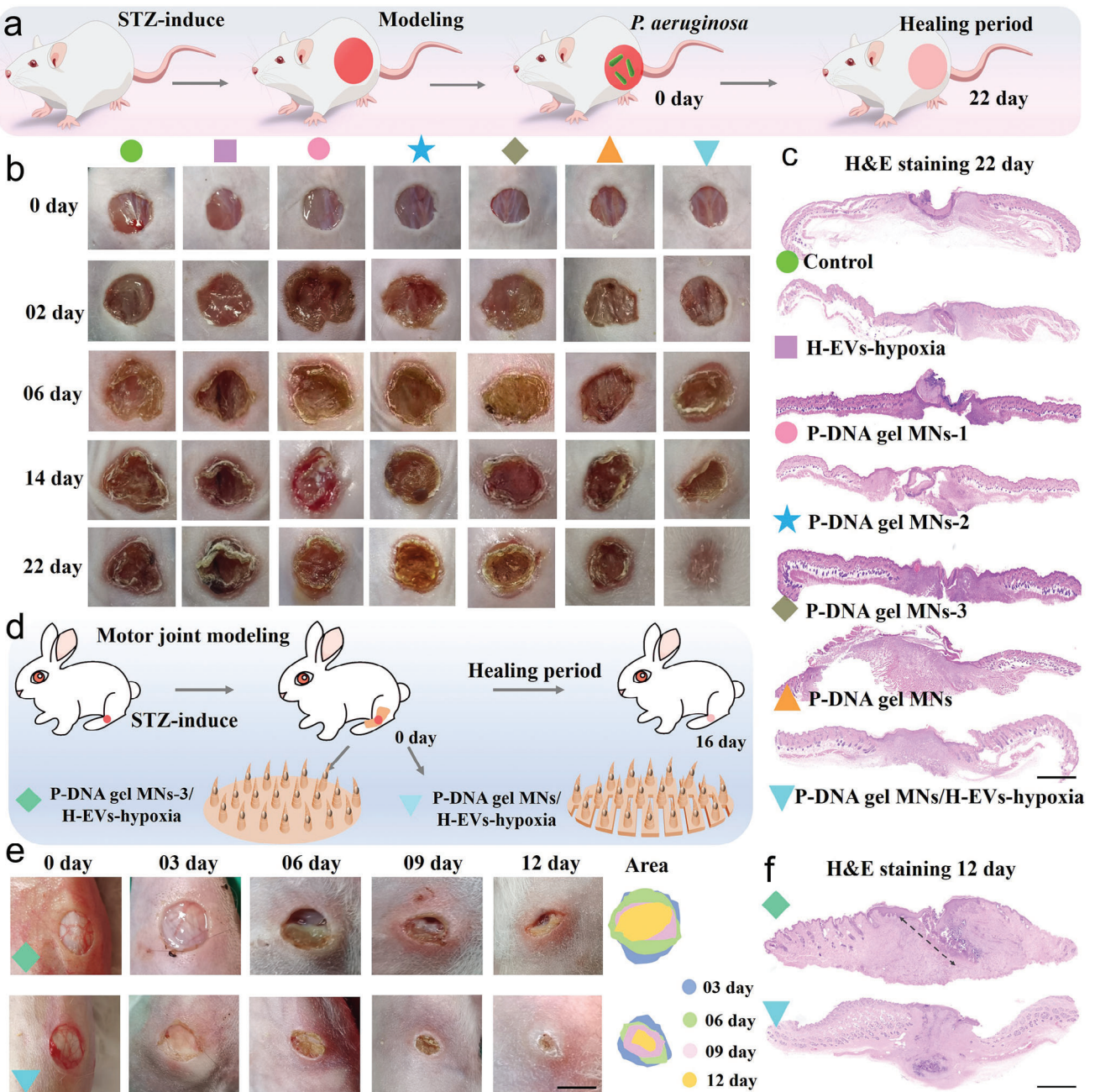


Figure 3. Establishment and treatment of wound. a) Establishment and treatment of infected wound in diabetes. b) Representative photos of infectious wounds. c) Wound tissue sections in different groups stained by H&E on days 22 (Scale bar: 1 mm). d) Establishment and treatment of joint wound in rabbits. e) Representative photos of joint wound in rabbits and statistical chart of wound cross section (Scale bar: 6 mm). f) Wound tissue sections in different groups stained by H&E on days 12 (Scale bar: 1 mm).

in the other groups were still unhealed (Figures S34a–g and S35, Supporting Information). Re-epithelialization is the primary gold standard for wound healing.^[33–35a] To evaluate re-epithelialization and granulation tissue formation, we examined tissue sections on the 22nd day. P-DNA gel MNs/H-EVs-hypoxia showed relatively intact newborn epithelial tissue (Figure 3c), while control group remained unhealed. Remaining groups showed incomplete epithelialization (Figure S36, Supporting In-

formation). Overall, combining optimized structure, DNA functional materials, and nutrients was conducive to healing wounds.

Considering that the back wound cannot replace the joint wound, we established rabbit leg joint full-thickness skin injury model and explored the influence of MNs with large deformation and undeformed structures on wound healing (Figure 3d). We evaluated the antibacterial activity of the material in the joint wound (Figure S37a, Supporting Information).

P-DNA gel MNs/H-EVs-hypoxia group with large deformation structure demonstrated significant healing, with a wound closure rate of $98 \pm 0.3\%$ (12th day) (Figure 3e and Figure S37b, Supporting Information). In contrast, P-DNA gel MNs-3/H-EVs-hypoxia group without large-deformed structure required 26 days for complete healing, as confirmed by quantitative wound area measurements (Figure S38a,b, Supporting Information). P-DNA gel MNs/H-EVs-hypoxia group showed evidence of epithelialization and new granulation tissue, while the P-DNA gel MNs-3/H-EVs-hypoxia group without large deformation structure exhibited residual scabs and deep suppuration (Figure 3f and Figure S38c, Supporting Information). Although P-DNA gel MNs-3/H-EVs-hypoxia group exhibited essential healing after 26 days, we still observed ulceration in deep tissue when we removed the wound tissue. H&E and Masson staining revealed the presence of necrotic tissue in the dermis (Figure S38d, Supporting Information). Overall, the elastic deformation generated by the MN with large deformation can not only meet the comfort of joint wound but promote high-quality wound healing.

2.7. Evaluation of the P-DNA Gel MNs Dressing Immune Regulation

Wound healing process involves immune regulation, re-epithelialization, and granulation tissue formation.^[36,37] Immune cells regulate the expression of wound microenvironment factors, judging the transition of wound from inflammation to remodeling stage.^[2] To assess whether P-DNA gel MNs/H-EVs-hypoxia can be directionally polarized, we initially cocultured material with LPS-induced RAW 264.7, with untreated RAW 264.7 used as control. After co-culturing cells and P-DNA gel MNs/H-EVs-hypoxia, we analyzed the differentially expressed genes (DEGs), which revealed that 1057, 51, and 1108 genes were upregulated, downregulated, and significantly expressed, respectively (Figure 4a). We subsequently performed hierarchical cluster analysis for the upregulated and downregulated genes, which showed different gene expression between control and P-DNA gel MNs/H-EVs-hypoxia groups (Figure S39a, Supporting Information). Specifically, genes expression related to anti-inflammatory polarizing factor and wound healing (FN1, IL-10, IL-33, and serpine1) were upregulated after P-DNA gel MNs/H-EVs-hypoxia (Figure 4b and Table S1, Supporting Information). Upregulated and downregulated genes were predominantly associated with the inflammatory phase and tended to exhibit an anti-inflammatory trend. Kyoto Encyclopedia of Genes and Genomes (KEGG) pathway enrichment analysis revealed that P-DNA gel MNs/H-EVs-hypoxia treatment enhanced cytokine-cytokine receptor interaction, Chemokine signaling pathway, TNF signaling pathway, IL-17 signaling pathway, JAK-STAT signaling pathway, and PI3K-Akt signaling pathway, which decreased inflammation and promoted wound healing (Figure 4c and Figures S39b and S40, and Table S1, Supporting Information).

Although TNF can activate inflammation and necrosis cascade,^[38,39] P-DNA gels MNs attenuated or hindered the harmful microenvironment by inhibiting the TNF signal. To further validate the effectiveness of RAN single-cell sequencing, we conducted double confirmation using WB and ELISA to ex-

plore how these materials regulate macrophage polarization. WB results indicate that the P-DNA gel MNs/H-EVs-hypoxia has significant anti-inflammatory effects (Figure S41a,b, Supporting Information). Compared with the control group ($176.0 \pm 0.667 \text{ pg mg}^{-1}$), the proinflammatory chemokine (TNF- α , $125.0 \pm 0.233 \text{ pg mg}^{-1}$, Figure S41c, Supporting Information) was significantly reduced after the P-DNA gel MNs/H-EVs-hypoxia treatment, indicating that material could inhibit inflammation. Furthermore, the expression levels of anti-inflammatory cytokines^[39a] IL-33 and IL-10 were 1.2 and 1.5 times higher in the P-DNA gel MNs group than in the control group (Figure S41d,e, Supporting Information), demonstrating that it effectively promoted the transformation of macrophages from M1 to M2 phenotype.

Based on the above in vitro conclusions, we further verified the polarization of inflammation. The protein expression of immunohistochemistry IL-1 β gradually decreased as we optimized functional materials' structure (Figure S42a, Supporting Information). P-DNA gel MNs/H-EVs-hypoxia group had the lowest IL-1 β protein expression, which was almost undetectable on the 9th day (Figure S42b, Supporting Information). RT-qPCR results also confirmed a significant decrease in the relative mRNA expression of IL-1 β (Figure 4d). P-DNA gel MNs group showed 1.3~1.5 times higher expression of IL-10 mRNA compared to other three groups without bionic and deformation structures (Figure 4e). P-DNA gel MNs/H-EVs-hypoxia group had almost 3.2~3.6 times higher expression of IL-10 mRNA compared to control group. Moreover, P-DNA gel MNs/H-EVs-hypoxia exhibited the highest IL-10 protein expression (Figure S43, Supporting Information).

To confirm that optimized materials with suitable structure and nutrients could promote polarization from M1 to M2 phenotype, we evaluated the protein expression of representative CD86 and CD206. On the 9th day, compared with the control group, the fluorescence intensity of CD86 in the P-DNA gel MNs group was relatively diminished because it could absorb excess exudate fluid and optimized structure reduce inflammation^[39b] (Figure 4f). Conversely, in the untreated control group, most macrophages retained the M1 phenotype (Figure S44a, Supporting Information). As expected, P-DNA gel MNs/H-EVs-hypoxia group had the highest fluorescence intensity of CD206 (Figure S44b, Supporting Information), demonstrating integrated system dressing, which combines functional DNA materials, optimized structure, and nutrients, to modulate immune activity, reduce inflammation, release repair factors, and promote transformation into remodeling period.

2.8. Evaluation of the P-DNA Gel MNs/EV-Hypoxia Neuroimmune Regulation

Macrophages play dual role in determining the pathogenesis of pain by inducing pain through interaction with peripheral pain receptor neurons and alleviating pain.^[40~42] Macrophages produced proinflammatory cytokines and chemokines, such as TNF- α , IL-1 β , IL-6, and CCL2, and Trpv1 were activated to trigger nociceptor-mediated pain response.^[40~43] The activation of Trpv1 can cause pain, burning, and itching, as well as the release of pro-inflammatory mediators such as substance P (SP) and

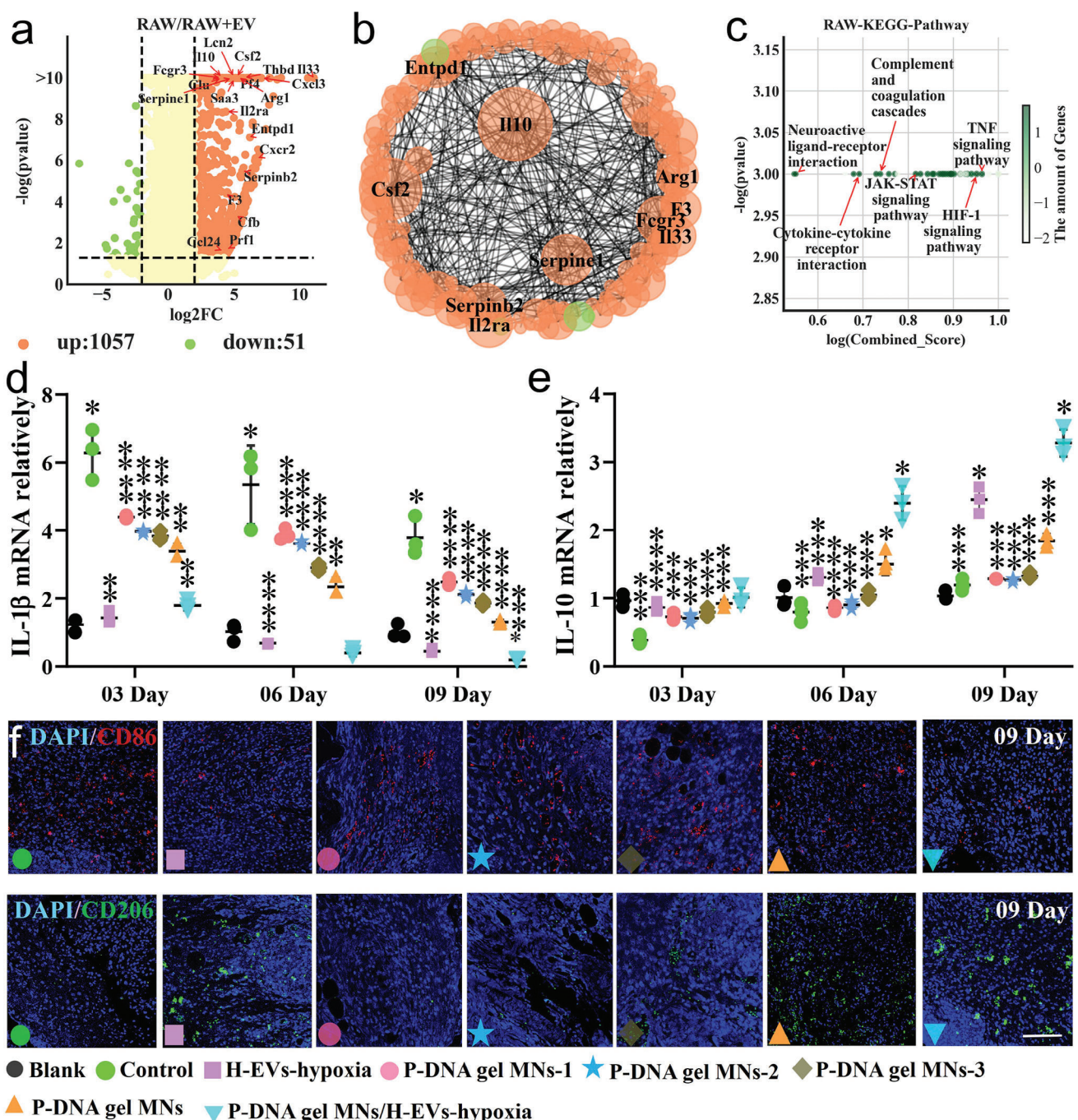


Figure 4. Characteristics of inflammatory regulation. a) The upregulated and downregulated genes in response to P-DNA gel MNs/EV-hypoxia treatment. b) Protein–protein interaction network. c) KEGG-Pathway enrichment analysis of the upregulated genes. d, e) IL-1 β and IL-10 expression of mRNA ($n = 3$, (*) $p < 0.1$, (**) $p < 0.01$, (***) $p < 0.001$, and (****) $p < 0.0001$ versus control group). f) CD86 and CD206 immunofluorescence staining (Scale bar: 200 μ m).

calcitonin gene related peptide (CGRP), mediating neurogenic inflammation and ultimately leading to the occurrence of various skin diseases and itching.^[44] To further explore the mechanism of inflammation-mediated pain, we preliminarily evaluated the relationship between inflammation and neuropathic pain through cocultured P-DNA gel MNs/EV-hypoxia and Trpv1

activation in SC.^[43] DEGs showed that 154, 130, and 24 genes were significantly expressed, upregulated, and downregulated, respectively (Figure 5a). Based on the enrichment analysis of upregulated and downregulated genes by DEGs, we screened different gene expression (Figure S4a, Supporting Information). Protein-protein interactions network analysis identified

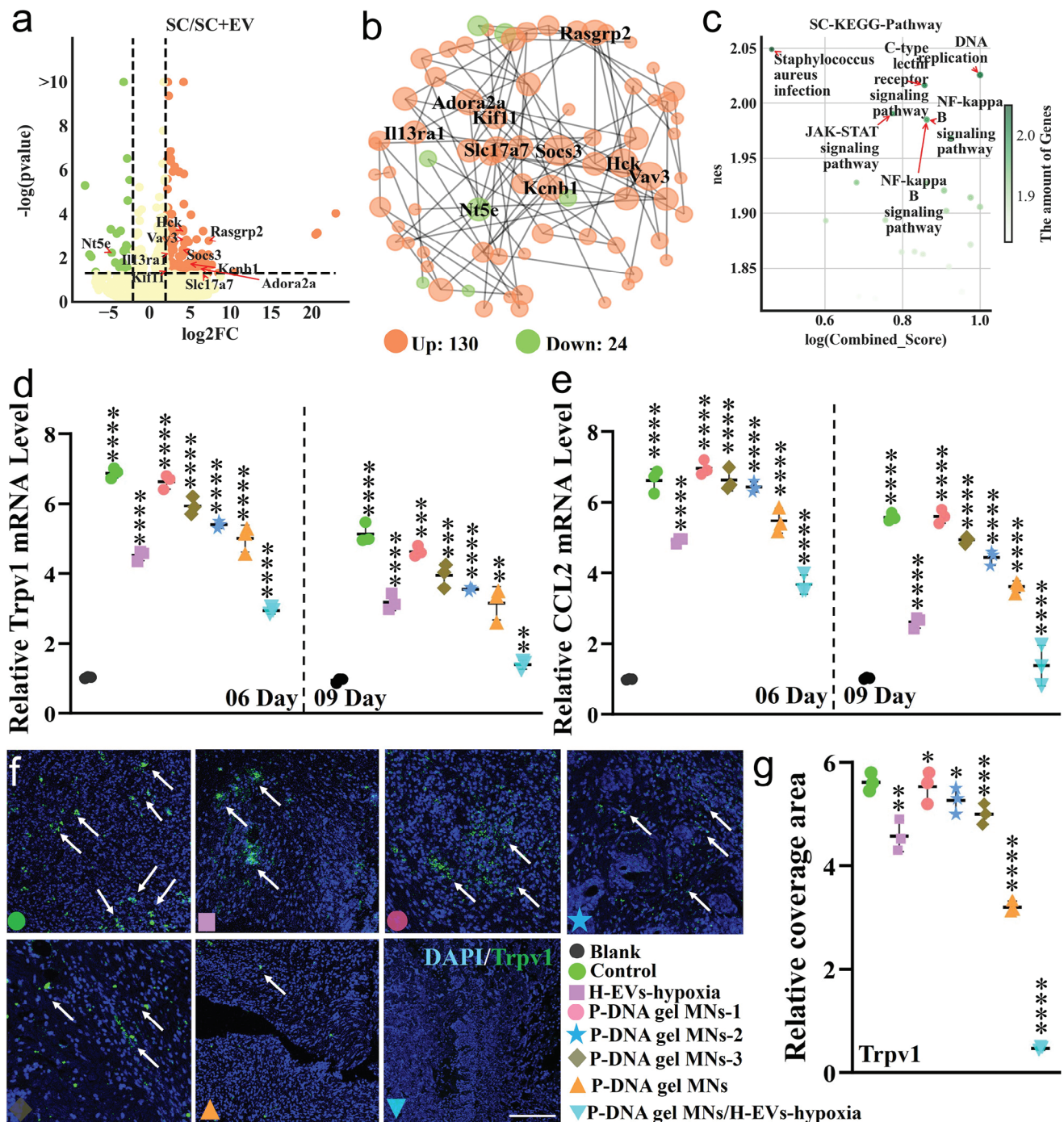


Figure 5. Inflammation-mediated neuralgia and neuroimmune regulation. a) Volcano plots showing the genes in response to P-DNA gel MNs/EV-hypoxia and SC co-culture. b) Protein–protein interaction network of upregulated and downregulated genes. c) KEGG-Pathway enrichment analysis of the upregulated genes. d,e) Effects of different materials on the expression of Trpv1 and CCL2 ($n = 3$). f) Trpv1 immunohistochemistry staining (Scale bar: 200 μ m). g) Trpv1 relative coverage area ($n = 3$). (*) $p < 0.1$, (**) $p < 0.01$, (***) $p < 0.001$ and (****) $p < 0.0001$.

that adjacent Socs3, HEK, IL33ra1, and Adora2a had the effect on regulating immune function and pain regulation in response to P-DNA gel MNs/EV-hypoxia treatment (Figure 5b). KEGG analysis showed that the key enrichment items focused on regulating immunity, ameliorating inflammation, and inhibiting pain. Among them, the mediated pathways related to inflammation

and pain, such as the Synaptic vesicle cycle, C-type lectin receptor signaling pathway, JAK-STAT signaling pathway, and NF- κ B signaling pathway. This confirmed that direct regulation of immune response mediated inflammation reduction and inhibited pain (Figure 5c and Figures S45b and S46, and Table S2, Supporting Information).

After tissue injury or infection, macrophages produce inflammatory mediators that can directly stimulate nociceptors and cause pain.^[43] To further explore inflammation and pain mechanisms, we evaluated inflammatory factors of tissues by ELISA. Inflammatory factors of P-DNA gel MNs with double biomimetic and large deformation were significantly lower than those without biomimetic structure (Figure S47a,b, Supporting Information). Furthermore, inflammatory factors expression was the lowest in the P-DNA gel MNs/H-EV-hypoxia, which was almost reduced 2.5–3 times that in the control group on the 9th day. Chronic wounds were prone to infection, accompanied by many oxidants, which aggravated inflammation and induced neuropathic pain.^[44–46] The common inflammatory pain signal factors were Trpv1 and CCL2.^[44–47a] We found that the mRNA expression of Trpv1 and CCL2 decreased gradually with the optimization of MNs structure design (Figure 5d,e). P-DNA gel MNs/H-EVs-hypoxia treatment significantly also decreased the expression level of Trpv1 to 1.39 ± 0.2 , significantly lower than that in the untreated control group (5.13 ± 0.9). The lowest expression of CCL2 in the P-DNA gel MNs/H-EVs-hypoxia treatment (1.37 ± 0.8) indicated that pain was effectively inhibited. To further verify the inhibitory effect of P-DNA gel MNs/H-EVs-hypoxia on neuralgia, we evaluated the protein expression of Trpv1 by immunofluorescence staining. The fluorescence intensity of Trpv1 was significantly decreased after P-DNA gel MNs/H-EVs-hypoxia treatment (Figure 5f,g). Additionally, the evaluation results of ELISA and RT-qPCR showed that the expression of SP was the lowest after treatment with P-DNA gel MNs/H-EVs-hypoxia, which was 8.9 pg mg^{-1} (ELISA: concentration) (Figure S48a, Supporting Information) and 0.79 (RT-qPCR: mRNA level) (Figure S48b, Supporting Information), respectively. The above results showed that P-DNA gel MNs/H-EVs-hypoxia system did have the effect of reducing inflammation and inhibiting pain.

2.9. P-DNA gel MNs/H-EVs-Hypoxia Promoting Wound Regeneration

Wound healing was closely related to various types of cells, including fibroblasts, macrophages, vascular endothelial, and nerve cells.^[47b] To gain a deeper understanding of wound healing and regeneration acceleration mechanisms, we co-cultured NHDF cells with P-DNA gel MNs/H-EVs-hypoxia and performed single-cell sequencing. Differential gene expression analysis identified 694 significantly different genes in NHDF cells treated with P-DNA gel MNs/H-EVs-hypoxia compared to NHDF cells that were not treated (Figure 6a). Protein-protein interaction network analysis (Figure 6b) revealed that genes such as CXCL10, CXCL11, MMP9, and MMP1 had significant impact on cell growth, angiogenesis, neurogenesis, and tissue remodeling. KEGG analysis showed that upregulated and downregulated genes were focused on cell proliferation and tissue remodeling (Figure S49a, Supporting Information).

During wound healing, proteases (including Matrix metalloproteinases (MMPs)) were closely related to cell migration after tissue injury, ECM remodeling, and epidermal repair.^[37,47c] Specifically, MMP3 and MMP9 were essential for wound re-epithelialization and epithelial migration.^[47c] We monitored the expression of protease (MMP3 and MMP9). The expression

of MMP3 and MMP9 was significantly lower in the P-DNA gel MNs/H-EVs-hypoxia group, which showed that P-DNA gel MNs/H-EVs-hypoxia treatment was conducive to cell migration and re-epithelialization (Figure 6c and Figure S49b,c, Supporting Information). KEGG pathway enrichment analysis revealed that P-DNA gel MNs/H-EVs-hypoxia treatment enhanced the signal transduction of the ECM-receptor interaction, cytokine–cytokine receptor interaction, and Chemokine signaling pathway (Figures S49d and S50, Supporting Information), which maintained the structure and function of cells and tissues, and provided basic guarantee for wound healing. Collagen synthesized by fibroblasts was the main component of the extracellular matrix.^[48] After P-DNA gel MNs/H-EVs-hypoxia treatment, ECM-receptor interaction signal pathway was upregulated (Table S3, Supporting Information). To further explore wound healing, we evaluated Collagen I and Collagen III expression (Figure 6d). Collagen III protein expression in the P-DNA gel MNs/H-EVs-hypoxia group gradually decreased (Figure S51a, Supporting Information), while Collagen I protein expression gradually increased (Figure S51d, Supporting Information), indicating that MNs system promotes collagen deposition the wound and tissue reconstruction.

During the proliferation phase, new blood vessels provide nutrition and oxygen for skin regeneration.^[49] To investigate the mechanism of angiogenesis at a cellular level, we performed RNA-seq analysis, which revealed 1810 upregulated and 425 downregulated genes (Figure 6e). Protein-protein interaction network analysis was performed to identify the gene, such as DCN, LUM, THBS2, COL1A1, and TIMP3, with a highly influential on cell migration, cell growth, angiogenesis, and tissue repair (Figure 6f). KEGG analysis revealed that the upregulated and downregulated genes focused on angiogenesis and wound healing. KEGG pathway enrichment analysis revealed that P-DNA gel MNs/H-EVs-hypoxia treatment enhanced signal transduction of Protein digestion and absorption, Calcium signaling pathway, Focal adhesion, PI3K-Akt signaling pathway, and Cytokine-cytokine receptor interaction (Figure 6g and Table S4, Figures S52a,b, and S53, Supporting Information).

Based on the above results, we further monitored the angiogenesis by the ELISA test (Figure S54, Supporting Information). As expected, VEGF protein content ($158.8 \pm 0.04 \text{ pg mL}^{-1}$) in the P-DNA gel MNs/H-EVs-hypoxia group was significantly higher compared to the control group ($91.1 \pm 0.03 \text{ pg mL}^{-1}$), H-EVs-hypoxia group ($113.5 \pm 0.06 \text{ pg mL}^{-1}$), P-DNA gel MNs-1 groups ($66.9 \pm 0.06 \text{ pg mL}^{-1}$), P-DNA gel MNs-2 groups ($57.1 \pm 0.04 \text{ pg mL}^{-1}$), P-DNA gel MNs-3 groups ($72.3 \pm 0.01 \text{ pg mL}^{-1}$), and P-DNA gel MNs groups ($135.1 \pm 0.03 \text{ pg mL}^{-1}$), respectively. This demonstrated that MNs system effectively upregulated angiogenesis of regenerated tissue. To validate angiogenesis, we conducted CD31 and α -SMA. As the structure improved, the fluorescent expression of CD31 gradually increased (Figure S55, Supporting Information). Although red fluorescence of CD31 was also detected in the P-DNA gel MNs group, its intensity was much lower than that in the P-DNA gel MNs/H-EVs-hypoxia (Figure S56a, Supporting Information). Relative expression of α -SMA was also consistent (Figure 6h and Figure S56b, Supporting Information). P-DNA gel MNs/H-EVs-hypoxia dressing with optimized structure and nutrients efficiently activated beneficial pathways and promoted angiogenesis regeneration.

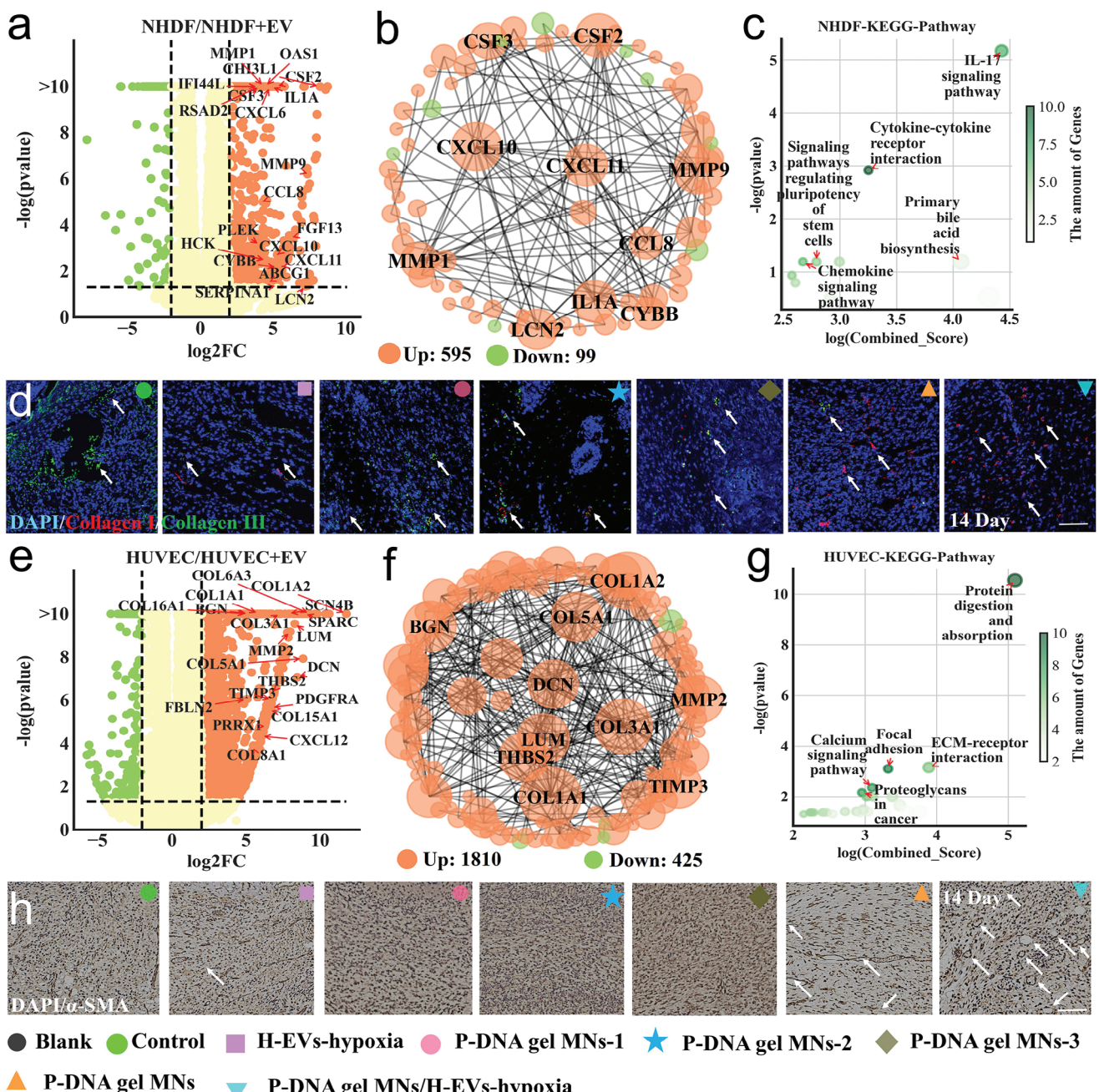


Figure 6. Mechanism of the P-DNA gel MNs/H-EVs-hypoxia promoting wound healing and regeneration. a) Volcano plots showing the genes in response to P-DNA gel MNs/EV-hypoxia and NHDF cells co-culture. b) Protein–protein interaction network of genes involved in wound healing and regeneration. c) KEGG analysis of the upregulated genes. d) Collagen I and Collagen III immunofluorescence staining (Scale bar: 200 µm). e) Volcano plots showing genes in response to P-DNA gel MNs/H-EVs-hypoxia and HUVEC co-culture. f) Protein–protein interaction network of genes involved in wound angiogenesis. g) KEGG analysis of the upregulated genes. h) Cα-SMA immunohistochemistry staining (Scale bar: 200 µm).

3. Conclusion

Inspired by crab grasp, shark microgroove, and Chinese paper-cut technology, we have successfully developed P-DNA gel MNs dressing with double bionics structures and large deformation to promote the repair and regeneration of diabetes wounds. P-DNA gel MNs were synthesized by entanglement between base

pairing, chemical crosslinking, and dense hydrogen bonds. The obtained P-DNA gel MNs have unique structure characteristics, such as proper grip, stability, and large deformation. Additionally, the loaded H-EVs-hypoxia endowed P-DNA gel MNs with anti-oxidation, anti-inflammatory, reducing pathological pain, and promoting nerve and angiogenesis. Notably, P-DNA gel MNs dressings with optimized structure and nutrients could activate

beneficial pathways to regulate wound microenvironment and thus encourage tissue regeneration. In conclusion, DNA MNs integrated system provides practical and effective strategy for treating chronic wounds and lays a foundation for further transformation of clinical medicine.

4. Experimental Section

The experimental details are provided in the Supporting Information.

Statistical Analyses: SPSS 20.0 software (IBM, USA) and GraphPad (GraphPad Prism Software Inc., San Diego, CA, USA) was used for statistical analysis of data. Each experiment was performed at least three times ($n \geq 3$), and data were shown as means \pm standard deviation. All data were shown as means \pm standard deviations (SD) using one-way ANOVA and the least significant difference (LSD) t-test. A p-value < 0.05 was denoted as statistically significant: (*) $p < 0.05$, (**) $p < 0.01$, (***) $p < 0.001$, and (****) $p < 0.001$.

Supporting Information

Supporting Information is available from the Wiley Online Library or from the author.

Acknowledgements

The adhesion of DNA gel MN dressings was tested on human participants who provided their informed written consent (**Volunteer Consent Statement**). The experiment involved human skin adhesion and was approved by the Ethics Committee of Peking University People's Hospital. All animal experiments were conducted in accordance with the regulations on animal management of the Ministry of health of the People's Republic of China and approved by animal care institutions. In addition, the experimental scheme was approved by the animal ethics committee of Peking University People's Hospital and implemented in accordance with the guidelines for experimental animals for ethical review of animal welfare in China (GB/T 35892-2018) (Ethics Committee/IACUC approval No.: 2019PHE027 and 2020PHE040). BALB/c mice (Specific pathogen Free, SPF) (male, 5–6 weeks) were purchased from Beijing Weitong Lihua Experimental Animal Technology Co., Ltd., (Beijing, China). New Zealand rabbit (male, 3.5 kg) were purchased from the Beijing the Longan experimental animal breeding center (Beijing, China). This work was supported by the National Natural Science Foundation of China (52273120, 21975019, and 22005012), National Science Foundation of Beijing (2172039, 7212121, and 2232037), China National Postdoctoral Program for Innovative Talents (BX20230039), China Postdoctoral Science Foundation (2023M740220), National Center for Trauma Medicine (BMU2020xy005-01), Laboratory of Advanced Materials and Green Manufacturing (Yantai) (AMGM2023F04) by the Science Fund of Shandong, Interdisciplinary Research Project for Young Teachers of USTB (FRF-IDRY-21-015), and the Fundamental Research Funds for the Central Universities and University of Science and Technology Beijing (USTB).

Conflict of Interest

The authors declare no conflict of interest.

Author Contributions

L.Z., Z.Z., and J.L. share co-first authorship. L.Z. performed investigation; designed the methodology; wrote the original draft; and visualized the

idea for study. Z.Z. and J.L. designed the methodology; performed investigation; and visualized the idea for study. F.Z., X.B., and Z.L. designed the methodology; and performed investigation. H.D. performed supervision; and wrote, reviewed, and edited the manuscript. P.Z. and Y.W. performed supervision and funding acquisition; conceptualized the idea for this study; and wrote, reviewed, and edited the manuscript.

Data Availability Statement

Research data are not shared.

Keywords

bionics structures, chinese paper-cutting technology, DNA hydrogel microneedles, extracellular vesicles, inflammatory polarization, tissue regeneration

Received: October 10, 2023

Revised: November 16, 2023

Published online: December 22, 2023

- [1] a) H. Chen, Y. Cheng, J. Tian, P. Yang, X. Zhang, Y. Chen, Y. Hu, J. Wu, *Sci. Adv.* **2020**, 6, eaba4311; b) A. M. Carracher, P. H. Marathe, K. L. Close, *J. Diabetes* **2018**, 10, 3531; c) J. Xiao, S. Chen, J. Yi, H. F. Zhang, G. A. Amer, *Adv. Funct. Mater.* **2017**, 27, 1604872.
- [2] a) L. Zhou, W. Pi, S. Cheng, Z. Gu, K. Zhang, T. Min, W. Zhang, H. Du, P. Zhang, Y. Wen, *Adv. Funct. Mater.* **2021**, 31, 2106167; b) Y. Guan, H. Niu, Z. Liu, Y. Dang, J. Shen, M. Zayed, L. Ma, J. Guan, *Sci. Adv.* **2021**, 7, eabj0153.
- [3] K. I. Ko, A. Sculean, D. T. Graves, *Transl. Res.* **2021**, 236, 72.
- [4] A. K. Gaharwar, I. Singh, A. Khademhosseini, *Nat. Rev. Mater.* **2020**, 5, 686.
- [5] M. Wang, C. Wang, M. Chen, Y. Xi, W. Cheng, C. Mao, T. Xu, X. Zhang, C. Lin, W. Gao, Y. Guo, B. Lei, *ACS Nano* **2019**, 13, 10279.
- [6] Y. Hu, B. Wu, Y. Xiong, R. Tao, A. C. Panayi, L. Chen, W. Tian, H. Xue, L. Shi, X. Zhang, L. Xiong, B. Mi, G. Liu, *Chem. Eng. J.* **2021**, 426, 130634.
- [7] S. Huang, P. Kuri, Y. Aubert, M. Brewster, N. Li, O. Farrelly, G. Rice, H. Bae, S. Prouty, T. Dentchev, W. Luo, B. C. Capell, P. Rompolas, *Cell Stem Cell* **2021**, 28, 1582.
- [8] a) X. Yao, W. Wei, X. Wang, L. Chenglin, M. Björklund, H. Ouyang, *Biomaterials* **2019**, 224, 119492; b) R. Kalluri, V. S. Lebleu, *Science* **2020**, 367, eaau6977; c) H. Kim, S. Y. Wang, G. Kwak, Y. Yang, I. C. Kwon, S. H. Kim, *Adv. Sci.* **2019**, 6, 1900513.
- [9] a) K. Zhang, X. Jiao, L. Zhou, J. Wang, C. Wang, Y. Qin, Y. Wen, *Biomaterials* **2021**, 276, 121040; b) L. P. Zhou, X. Jiao, S. Liu, M. Hao, S. Cheng, P. Zhang, Y. Wen, *J. Mater. Chem. B* **2020**, 8, 1991.
- [10] Y. Dong, C. Yao, Y. Zhu, L. Yang, D. Luo, D. Yang, *Chem. Rev.* **2020**, 120, 9420.
- [11] L. Zhou, Z. Zeng, S. Liu, T. Min, W. Zhang, X. Bian, H. Du, P. Zhang, Y. Wen, *Adv. Funct. Mater.* **2022**, 32, 2207466.
- [12] F. Li, J. Tang, J. Geng, D. Luo, D. Yang, *Prog. Polym. Sci.* **2019**, 98, 101163.
- [13] a) C. Yao, H. Tang, W. Wu, J. Tang, W. Guo, D. Luo, D. Yang, *J. Am. Chem. Soc.* **2020**, 142, 3422; b) F. Li, D. Lyu, S. Liu, W. Guo, *Adv. Mater.* **2020**, 32, 1806538.
- [14] T. Yuan, Y. Shao, X. Zhou, Q. Liu, Z. Zhu, B. Zhou, Y. Dong, N. Stephanopoulos, S. Gui, H. Yan, D. Liu, *Adv. Mater.* **2021**, 33, 2102428.
- [15] a) M. Malone, G. Schultz, *Br. J. Dermatol.* **2022**, 187, 159; b) F. C. Wells, S. W. B. Newsom, C. Rowlands, *Lanc* **1983**, 321, 1209.

- [16] Y. Sun, J. Liu, H. Wang, S. Li, X. Pan, B. Xu, H. Yang, Q. Wu, W. Li, X. Su, Z. Huang, X. Guo, H. Liu, *Adv. Funct. Mater.* **2021**, *31*, 2100218.
- [17] L. Zhou, T. Min, X. Bian, Y. Dong, P. Zhang, Y. Wen, *ACS Appl. Bio Mater.* **2022**, *5*, 4055.
- [18] Q. Zhang, L. Shi, H. He, X. Liu, Y. Huang, D. Xu, M. Yao, N. Zhang, Y. Guo, Y. Lu, H. Li, J. Zhou, J. Tan, M. Xing, G. Luo, *ACS Nano* **2022**, *16*, 10163.
- [19] Y. Deng, C. Yang, Y. Zhu, W. Liu, H. Li, L. Wang, W. Chen, Z. Wang, L. Wang, *Nano Lett.* **2022**, *22*, 2702.
- [20] a) X. Zhang, G. Chen, Y. Yu, L. Sun, Y. Zhao, *Research* **2020**, *2020*, 3672120; b) J. Tang, J. Wang, K. Huang, Y. Ye, T. Su, L. Qiao, M. T. Hensley, T. G. Caranasos, J. Zhang, Z. Gu, K. Cheng, *Sci. Adv.* **2018**, *4*, eaat9365. c) X. Zhang, G. Chen, L. Sun, F. Ye, X. Shen, Y. Zhao, *Chem. Eng. J.* **2021**, *406*, 126741; d) Q. Zhang, H. Dong, Y. Li, Y. Zhu, L. Zeng, H. Gao, B. Yuan, X. Chen, C. Mao, *ACS Appl. Mater. Interface* **2015**, *41*, 23336; e) N. Zhao, S. Yin, S. Xie, H. Yan, P. Ren, G. Chen, F. Chen, J. Xu, *Angew. Chem., Int. Ed.* **2018**, *57*, 3520.
- [21] M. Wang, Y. Han, X. Yu, L. Liang, H. Chang, D. C. Yeo, C. Wiraja, M. L. Wee, L. Liu, X. Liu, C. Xu, *Adv. Healthcare Mater.* **2020**, *9*, 1900635.
- [22] S. P. Sullivan, D. G. Koutsonanos, M. P. Martin, J. W. Lee, V. Zarnitsyn, S. Choi, N. Murthy, R. W. Compans, I. Skountzou, M. R. Prausnitz, *Nat. Med.* **2010**, *16*, 915.
- [23] J. D. Watson, F. H. C. Crick, *Nature* **1953**, *171*, 737.
- [24] a) G. Pan, F. Li, S. He, W. Li, Q. Wu, J. He, R. Ruan, Z. Xiao, J. Zhang, H. Yang, *Adv. Funct. Mater.* **2022**, *32*, 2200908; b) K. Kim, J. H. Ryu, M.-Y. Koh, S. P. Yun, S. Kim, J. P. Park, C.-W. Jung, M. S. Lee, H.-I. Seo, J. H. Kim, H. Lee, *Sci. Adv.* **2021**, *7*, eabc9992; c) X. Liu, Q. Zhang, Z. Gao, R. Hou, G. Gao, *ACS Appl. Mater. Interfaces* **2017**, *9*, 17645; d) Y. Shen, G. Xu, H. Huang, K. Wang, H. Wang, M. Lang, H. Gao, S. Zhao, *ACS Nano* **2021**, *15*, 6352.
- [25] K. O'brien, K. Breyne, S. Ughetto, L. C. Laurent, X. O. Breakefield, *Nat. Rev. Mol. Cell. Biol.* **2020**, *21*, 585.
- [26] Y. Zhang, Z. Hao, P. Wang, Y. Xia, J. Wu, D. Xia, S. Fang, S. Xu, *Cell Prolif.* **2019**, *52*, e12570.
- [27] Y. Zhu, Y. Jia, Y. Wang, J. Xu, Y. Chai, *Stem Cells Transl. Med.* **2019**, *8*, 593.
- [28] a) A. Casado-Díaz, J. M. Quesada-Gómez, G. Dorado, *Front. Bioeng. Biotechnol.* **2020**, *8*, 146; b) D. M. Pegtel, S. J. Gould, *Annu Rev. Biochem.* **2019**, *88*, 487; c) P. Zhao, Y. Feng, Y. Zhou, C. Tan, M. Liu, *Bioact. Mater.* **2023**, *20*, 355.
- [29] N. Tang, R. Zhang, Y. Zheng, J. Wang, M. Khatib, X. Jiang, C. Zhou, R. Omar, W. Saliba, W. Wu, M. Yuan, D. Cui, H. Haick, *Adv. Mater.* **2022**, *34*, 2106842.
- [30] X. Yang, C. Ding, M. Wu, X. Xu, X. Ke, H. Xu, J. Li, F. Lou, K. Zhou, H. Jiang, X. Peng, X. Wang, L. Si, J. Li, *Chem. Eng. J.* **2021**, *415*, 128955.
- [31] a) L. Cheng, Z. Cai, T. Ye, X. Yu, Z. Chen, Y. Yan, J. Qi, L. Wang, Z. Liu, W. Cui, L. Deng, *Adv. Funct. Mater.* **2020**, *30*, 2001196; b) H. Xu, Z. Fang, W. Tian, Y. Wang, Q. Ye, L. Zhang, J. Cai, *Adv. Mater.* **2018**, *30*, 180110.
- [32] Y. Yu, P. Li, C. Zhu, N. Ning, S. Zhang, G. J. Vancso, *Adv. Funct. Mater.* **2019**, *29*, 1904402.
- [33] A. Liu, Q. Wang, Z. Zhao, R. Wu, M. Wang, J. Li, K. Sun, Z. Sun, Z. Lv, J. Xu, H. Jiang, M. Wan, D. Shi, C. Mao, *ACS Nano* **2021**, *15*, 13339.
- [34] B. Hu, W. R. Leow, S. Amini, B. Nai, X. Zhang, Z. Liu, P. Cai, Z. Li, Y.-L. Wu, A. Miserez, C. T. Lim, X. Chen, *Adv. Mater.* **2017**, *29*, 1700145.
- [35] a) G. Augustine, M. Aarthy, H. Thiagarajan, S. Selvaraj, N. R. Kamini, G. Shanmugam, N. Ayyadurai, *Adv. Healthcare Mater.* **2021**, *10*, 2001832; b) S. Liu, L. Yao, Y. Wang, Y. Jia, Y. Yang, N. Li, Y. Hu, D. Kong, X. Dong, K. Wang, M. Zhu, *Bioact. Mater.* **2023**, *21*, 464.
- [36] C. H. Su, S. H. Liu, S. Y. Yu, Y. L. Hsieh, H. Ho, C. H. Hu, M. T. Sheu, *Composites, Part A* **2005**, *72*, 220.
- [37] F.-Y. Hsu, Y.-S. Hung, H.-M. Liou, C.-H. Shen, *Acta Biomater.* **2010**, *6*, 2140.
- [38] G. Opdenakker, J. Van Damme, J. J. Vranckx, *Trend Immunol.* **2018**, *39*, 341.
- [39] a) D. R. Griffin, M. M. Archang, C.-H. Kuan, W. M. Weaver, J. S. Weinstein, A. C. Feng, A. Ruccia, E. Sideris, V. Ragkousis, J. Koh, M. V. Plakus, D. Di Carlo, T. Segura, P. O. Scumpia, *Nat. Mater.* **2021**, *20*, 560; b) S. Hauck, P. Zager, N. Halfter, E. Wandel, M. Torregrossa, A. Kakpenova, S. Rother, M. Ordieres, S. Rathel, A. Berg, S. Moller, M. Schnabelrauch, J. C. Simon, V. Hintze, S. Franz a, *Bioact. Mater.* **2021**, *6*, 4342.
- [40] O. Chen, C. R. Donnelly, R.-R. Ji, *Curr. Opin. Neurobiol.* **2020**, *62*, 17.
- [41] C. Bian, Z.-C. Wang, J.-L. Yang, N. Lu, Z.-Q. Zhao, Y.-Q. Zhang, *Brain. Behav. Immun.* **2014**, *37*, 220.
- [42] X. Luo, O. Chen, Z. Wang, S. Bang, J. Ji, S. H. Lee, Y. Huh, K. Furutani, Q. He, X. Tao, M.-C. Ko, A. Bortsov, C. R. Donnelly, Y. Chen, A. Nackley, T. Berta, R.-R. Ji, *Neuron* **2021**, *109*, 2691.
- [43] J. Sun, R. D. Ramnath, L. Zhi, R. Tamizhselvi, M. Bhatia, *AJP Cell Physiology* **2008**, *294*, C1586.
- [44] a) F. De Logu, R. Nassini, S. Materazzi, M. Carvalho Gonçalves, D. Nosi, D. Rossi Degl'innocenti, I. M. Marone, J. Ferreira, S. Li Puma, S. Benemei, G. Trevisan, D. Souza Monteiro De Araújo, R. Patacchini, N. W. Bennett, P. Geppetti, *Nat. Commun.* **2017**, *8*, 1887; b) X. Zhang, J. F. Wang, Y. Maor, G. Kunos, J. E. Groopman, *Blood* **2006**, *108*, 1808.
- [45] G. Trevisan, S. Benemei, S. Materazzi, F. De Logu, G. De Siena, C. Fusi, M. Fortes Rossato, E. Coppi, I. M. Marone, J. Ferreira, P. Geppetti, R. Nassini, *Brain* **2016**, *139*, 1361.
- [46] K. Obata, *J. Clin. Invest.* **2005**, *115*, 2393.
- [47] a) Y.-J. Gao, R.-R. Ji, *Pharmacol. Ther.* **2010**, *126*, 56; b) G. Theocharidis, H. Yuk, H. Roh, L. Wang, I. Mezghani, J. Wu, A. Kafanas, M. Contreras, B. Sumpio, Z. Li, E. Wang, L. Chen, C. F. Guo, N. Jayaswal, X. L. Katopodi, N. Kalavros, C. S. Nabzydk, I. S. VLachos, A. Veves, X. Zhao, *Nat. Biomed. Eng.* **2022**, *4*, 1118; c) M. R. K. Dasu, M. Spies, R. E. Barrow, D. N. Herndon, *Wound Repair Regen* **2003**, *11*, 177.
- [48] C. Zhou, Z. Yang, X. Xun, L. Ma, Z. Chen, X. Hu, X. Wu, Y. Wan, H. Ao, *Bioact. Mater.* **2022**, *13*, 212.
- [49] P. Lou, S. Liu, Y. Wang, C. Pan, X. Xu, M. Zhao, G. Liao, G. Yang, Y. Yuan, L. Li, J. Zhang, Y. Chen, J. Cheng, Y. Lu, J. Liu, *Acta Biomater.* **2021**, *135*, 100.